Hominoid-specific transposable elements rewired the expression of neural crest migration genes

Laura Deelen[1], Zoe H. Mitchell[1], Martina Demurtas[1], Andria Koulle[1], Beatriz Garcia Del Valle[1], and Marco Trizzino[1,*]

1 Department of Life Sciences, Imperial College London, SW7 2AZ London, UK

***Corresponding author**: E-mail: m.trizzino@imperial.ac.uk

Abstract

Craniofacial development is evolutionarily conserved, yet subtle changes in its regulatory network drive species-specific traits. Transposable elements (TEs) contribute to genome evolution, but their role in cranial neural crest cells (CNCCs) remains unclear. Here, we investigate the domestication of hominoid-specific TEs (LTR5Hs and SVAs) as enhancers during human CNCC specification, a process critical for vertebrate craniofacial development. Using human iPSC-derived CNCCs, we identified ~550 hominoid-specific TEs functioning as enhancers, including ~250 human-specific, predominantly LTR5Hs. These elements are enriched for CNCC coordinator motifs, are bound by the CNCC signature factor TWIST1, and their enhancer activity appears largely CNCC-specific. CRISPR-interference targeting ~75% of these active TEs led to widespread transcriptional dysregulation of genes involved in neural crest migration, and two orthogonal functional assays confirmed that CNCC migration is impaired upon TE repression. Finally, genes near human-specific TEs showed higher expression in human CNCCs compared to chimpanzee CNCCs, but TE repression restored gene expression to chimpanzee levels. These findings highlight how young TEs were domesticated to fine-tune CNCC regulatory networks, potentially contributing to lineage-specific craniofacial evolution.

Keywords: Cell migration / coordinator motif / Cranial Neural Crest / LTR5Hs / SVAs

Introduction

Craniofacial development is a highly complex process that requires precise spatiotemporal regulation and involves contributions from all three germ layers, and in particular from neural crest cells (NCCs) (Gans & Northcutt, 1983; Ahlstrom & Erickson, 2009; Martik & Bronner, 2021; Theveneau & Mayor, 2012). NCCs emerge during early embryogenesis, between weeks 3-4 in humans, at the neural plate border between the neuroectoderm and non-neural ectoderm. As neurulation progresses, the neural plate invaginates and separates from the dorsal ectoderm, forming the neural tube. At this stage, NCCs undergo epithelial-to-mesenchymal transition (EMT), allowing them to delaminate and migrate to specific regions throughout the developing embryo (Ahlstrom & Erickson, 2009; Martik & Bronner, 2021; Theveneau & Mayor, 2012). Among the NCC subtypes, cranial neural crest cells (CNCCs) play a pivotal role in the formation of key craniofacial structures, including bones and cartilage (Bronner & LeDouarin, 2012; Cordero et al., 2011; Jheon & Schneider, 2009).

Although craniofacial development is an evolutionary conserved process, recent adaptations to the modern human craniofacial complex include changes in shape and function to accommodate the enlargement of the brain, the transition to bipedal posture, laryngeal extension for speech as well as adjustments for the evolvement of sensory organs (Lieberman, 1998; Sambataro et al., 2022; Spoor et al., 1994). The evolution of human-specific craniofacial traits has required precise modifications in gene expression and increasing evidence suggests that regulatory changes, rather than protein-coding mutations, have been key to shaping species-specific features (Carroll, 2005; King & Wilson, 1975; Wray, 2007). One major source of these regulatory innovations are the transposable elements (TEs). Comprising nearly half of the human genome, TEs are now recognized as key contributors to genomic evolution through their ability to integrate into the genome and act as cis-regulatory elements (Bourque et al., 2008; Chuong et al., 2013, 2016; Cosby et al., 2021; Goubert et al., 2020; Kunarso et al., 2010; Lynch et al., 2011; Pontis et al., 2019; Schmidt et al., 2012; Sundaram & Wysocka, 2020). Transposable element-mediated rewiring of gene regulatory networks has previously been implicated as a major driver of species-specific gene expression patterns (Chuong et al., 2013; Feschotte, 2008; Fueyo et al., 2022; Jacques et al., 2013; Patoori et al., 2022; Playfoot et al., 2021; Prescott et al., 2015; Sundaram et al., 2014; Trizzino et al., 2017).

However, much remains to be uncovered about the precise mechanisms through which transposable elements (TEs) have been co-opted as cis-regulatory elements in humans, particularly in the context of craniofacial development. In the human genome, SINE-VNTR-Alus (SVAs) and LTR5Hs have been previously linked to gene regulatory activity (Barnada et al., 2022; Chuong et al., 2016; Fuentes et al., 2018; Patoori et al., 2022; Pontis et al., 2019; Trizzino et al., 2017). SVAs are the youngest TE family and include over 3000 copies in the human genome. They are composed of a hexamer repeat, an Alu-like element, a variable

number of tandem repeats (VNTRs), a SINE element, and a poly-A tail (Fig. 1A). The SVAs are hominoid-specific, comprise of six subfamilies (A–F), with SVA-E and SVA-F being found exclusively in humans, with ∼1700 copies in total (Quinn & Bubb, 2014; Wang et al., 2005). LTR5Hs are also human-specific and are remnants of an ancestral endogenous retrovirus of the HERV-K subtype.

Co-option of SVAs and LTR5Hs as active cis-regulatory elements has been observed in different human tissues (Barnada et al., 2022; Chuong et al., 2013; Fuentes et al., 2018; Ostertag et al., 2003; Patoori et al., 2022; Pontis et al., 2019; Trizzino et al., 2017). Since the expansion of LTR5Hs and SVA-E/F subfamilies occurred around the time of the human–chimpanzee split, we set out to investigate if these elements could have contributed to human-specific craniofacial development.

Human cranial neural crest cell (CNCC) specification and migration can be effectively modelled *in vitro* using human-induced pluripotent stem cells (hiPSCs). Therefore, in this study, we employed an inducible CRISPR-interference (CRISPRi) hiPSC line to investigate the impact of silencing human SVA and LTR5Hs elements to CNCC specification and migration, which are essential processes for the development of the craniofacial structures, including bones and cartilage. To achieve this, we employed previously published single-guide RNAs (sgRNAs) targeting approximately 80% of these transposable elements (Pontis et al., 2019).

With this approach, we identified approximately ~550 human SVAs and LTR5Hs that are accessible and depleted of the repressive histone mark H3K9me3 in human CNCCs. We found that the specific DNA sequence was the primary driver for the co-option of this set of TEs. Importantly, silencing these retroelements attenuated the expression of hundreds of genes involved in CNCC migration, which is a key process in craniofacial morphogenesis. Functional assays confirmed that migration was disrupted, suggesting a potential role for the transposons in species-specific craniofacial development. This was further supported by comparisons with previously published chimpanzee CNCC data, where the corresponding genes to those near accessible human-specific transposable elements showed expression patterns similar to those in human CNCCs when these elements were silenced.

Results

An inducible CRISPR-interference iPSC system for the repression of SVAs and LTR5Hs

To investigate the role of hominoid-specific TEs (SVAs and LTR5Hs; Fig. 1a) in human cranial neural crest cell (CNCC) development, we designed a stable human iPSC line with an inducible CRISPR-interference (CRISPRi) system with single-guide RNAs (sgRNAs) targeting ~80% of all SVAs and LTR5Hs annotated in the human genome (Fig. 1b). The sgRNAs were

102 originally designed and validated in a recent seminal study (Pontis et al., 2019) and were
103 further used in subsequent studies (Barnada et al., 2022; Patoori et al., 2022). Briefly, we
104 cloned a stable iPSC line with a permanently integrated TET-inducible, catalytically dead,
105 Cas9 fused to a repressive KRAB domain (dCas9-KRAB), along with the two gRNAs targeting
106 LTR5Hs and SVAs (hereafter +gRNA line). The KRAB domain recruits the transcriptional
107 machinery necessary to deposit repressive histone methylation (H3K9me3) to the regions
108 targeted by dCas9. To account for potential off-target effects caused by exposure to
109 doxycycline (TET-ON) or by Cas9 expression, we cloned the same iPSC line with an identical
110 dCas9-KRAB construct but without any gRNAs (hereafter -gRNAs line). Treating the cells with
111 doxycycline for 24 hours was sufficient to activate dCas9 in both CRISPRi lines (i.e. with and
112 without gRNAs; Fig. 1c,d).
113 Next, we generated CNCCs from our CRISPRi-iPSC lines using an established 5-day protocol
114 (Fig. 1e,f; Leung et al., 2016). Since both SVAs and LTR5Hs have been shown to have
115 important roles in human embryonic stem cells and iPSCs (Barnada et al., 2022; Fuentes et
116 al., 2018; Pontis et al., 2019), doxycycline was only introduced 24h after differentiation (Fig.
117 1c). By day 5 of differentiation, both cell lines expressed markers typical of CNCC identity,
118 both at gene (*SOX9*, *SOX10*, *TWIST1*, *TFAP2A*) and protein (SOX9, AP2α) level. We
119 generally did not observe significant differences in CNCC marker expression between the two
120 lines, apart from *TFAP2A* (Fig. 1e,f), indicating that expression of the main genes essential for
121 CNCC identity was largely unaffected by the CRISPRi with the exception of *TFAP2A*.
122 Finally, using RNA-seq data, we explored the TE expression landscape in human CNCCs.
123 This revealed that many TE subfamilies are highly expressed (including SVAs and HERVK-
124 LTRs, with Alu (SINE) and L1 (LINE) elements dominating (Appendix Fig. S1a, Appendix File.
125 S1).
126
127 **Hundreds of SVAs and LTR5Hs are accessible in human CNCCs**
128 We first set out to determine whether any SVA and LTR5Hs exhibited chromatin accessibility
129 in human CNCCs, and whether these elements could be repressed using our CRISPRi
130 system. To this end, we performed ATAC-seq (paired-end, 150 bp reads) in hiPSC-derived
131 CNCCs generated with our CRISPRi-iPSC lines (- and +gRNAs). We started by examining
132 human-specific SVAs (i.e. SVA-E, SVA-F) and LTF5Hs. K-mer clustering of the ATAC-seq data
133 identified a total of 256 accessible LTR5Hs and human-specific SVAs (Fig. 2a; Appendix File
134 S2). Notably, 77% of these 256 TEs displayed decreased accessibility in the +gRNA CRISPRi
135 line relative to the -gRNA control (cluster 2, Fig. 2a). This is consistent with the assumption
136 that these gRNAs can target ~80% of all the human LTR5Hs and SVAs (Pontis et al. 2019).
137 LTR5Hs were significantly overrepresented among the 256 accessible human-specific TEs

138 (observed 87%, expected 29%; Fisher's Exact Test $p < 2.2 \times 10^{-16}$; Fig. 2b), while the SVAs
139 were significantly underrepresented (13% observed vs 71% expected; Fisher's Exact Test $p <$
140 2.2×10^{-16}; Fig. 2b), highlighting a potential primary role for LTR5Hs in CNCCs.
141 We set out to confirm that the loss in chromatin accessibility observed in the +gRNA lines was
142 a direct consequence of the CRISPRi-mediated repression. To this end, we performed ChIP-
143 seq for H3K9me3 (paired-end 150 bp reads), which showed accumulation of this repressive
144 histone mark at approximately 75% of the 256 accessible LTR5Hs and human-specific SVAs
145 in the +gRNA samples (Fig. 2c). Notably, there was a remarkable overlap (92%) between the
146 TEs that lost chromatin accessibility (Fig. 2a) and those gaining H3K9me3 (Fig. 2c).
147 We further investigated the genomic locations of these accessible human-specific TEs.
148 Overall, 91% of the 256 accessible LTR5Hs and human-specific SVAs were located > 1 kb
149 from the nearest transcription start site (TSS), and the median distance was 8.9 kb (Appendix
150 Fig. S1b). This suggests that these accessible mobile elements could be putative CNCC
151 enhancers. To confirm this, we leveraged publicly available H3K27ac ChIP-seq data
152 previously generated by our group in hiPSC-derived CNCCs (Barnada et al., 2024; Data ref:
153 Barnada et al., 2024). This analysis revealed that the vast majority of the 256 accessible
154 human-specific TEs also displayed the H3K27ac modification, an established active enhancer
155 mark, supporting their role as bona-fide human-specific CNCC enhancers (Appendix Fig.
156 S1c).
157 To investigate whether these accessible human-specific TEs are actively transcribed in
158 CNCCs, we performed a H3K4me3 ChIP-seq (which is a marker for actively transcribing
159 promoters) in -gRNA CNCCs and +gRNA CNCCs. This experiment revealed that 39.5% of the
160 accessible LTR5Hs and human-specific SVAs were also decorated by H3K4me3, suggesting
161 that over a third of the accessible LTR5Hs and human-specific SVAs are likely engaged in
162 active transcription in CNCCs (Appendix Fig. S1d,e).
163 Next, we focused on the accessibility of all SVA subfamilies, including those that are also found
164 in other hominoid species (SVA_A, _B, _C, _D). To this end, we analysed the ATAC-seq signal
165 across all existing SVA subfamilies and LTR5Hs separately (Appendix Fig. S2a,b). This yielded
166 results consistent to the previous analysis, since we found that 5% (n = 258) of non-human-
167 specific SVAs (A–D subfamilies) were accessible in CNCCs, whilst 95% (n = 5716) were
168 inaccessible (Appendix Fig. S2a,b). Therefore, even when accounting for all SVA groups,
169 SVAs remained significantly underrepresented among accessible TEs.
170 In summary, these experiments identified approximately 550 hominoid-specific TEs, over half
171 of which human-specific, that exhibit signatures of active enhancers in human iPSC-derived
172 CNCCs, with LTR5Hs elements playing a prominent role. Notably, our CRISPR-based
173 approach enabled the inducible repression of ~75% of these putative TE-derived human-
174 specific CNCC enhancers.

175 To ensure that our findings were not biased by a specific differentiation protocol, we used an
176 alternative iPSC-to-CNCC differentiation method (Bajpai et al., 2010) and performed ATAC-
177 seq on the differentiated cells. With this protocol, migratory CNCCs are obtained in 2-3 weeks
178 (Bajpai et al., 2010; Barnada et al., 2024; Mitchell et al., 2025; Pagliaroli et al., 2021). Using
179 this approach, we identified 374 LTR5Hs and human-specific SVA elements that are
180 accessible in CNCCs, the majority of which exhibited reduced accessibility in the +gRNA line
181 compared to the -gRNA control (Appendix Fig. S2c). Moreover, comparable to our findings
182 obtained with the 5-day protocol, LTR5Hs were significantly overrepresented in the set of
183 accessible TEs (83% observed vs 29% expected; Fisher's Exact Test $p < 2.2 \times 10^{-16}$), while
184 SVAs were significantly underrepresented (17% observed vs 71% expected; Fisher's Exact
185 Test $p < 2.2 \times 10^{-16}$). Importantly, 91% of the 256 human-specific TEs identified as accessible
186 in the 5-day protocol were also found accessible in CNCCs derived using the alternative
187 protocol. This consistency suggests that our findings are robust and independent of the CNCC
188 differentiation method used.
189
190 **Co-opted TEs are enriched with the CNCC *coordinator* motif**
191 Next, we explored the genomic features driving the recruitment of the LTR5Hs and SVAs as
192 CNCC enhancers. First, we performed computational DNA motif analysis on the set of
193 accessible TEs using the non-accessible LTR5Hs and SVAs as background control for
194 differential enrichment. Recent studies have identified a specific DNA motif, known as
195 *coordinator*, which is enriched at enhancers critical for the regulation of CNCC identity (Kim et
196 al., 2024; Prescott et al., 2015). *Coordinator* is a composite motif which consists of a fusion
197 between a generic AT-rich homeobox motif (TTAATTA) and the binding motif of the CNCC
198 master regulator TWIST1, typically joined by a stretch of A nucleotides (Kim et al., 2024;
199 Prescott et al., 2015). Importantly, we found both components of the *coordinator motif* as highly
200 enriched in the set of accessible LTR5Hs and human-specific SVAs (Fig. 2d; Appendix File
201 S3). Specifically, the TWIST1 motif and the AT-rich homeobox motif were found in 83% and
202 62% of accessible human-specific TEs, respectively, with similar numbers observed when
203 incorporating non-human-specific SVAs in the analysis (Fig. 2d; Appendix Fig. 2d,e; Appendix
204 File S3). Moreover, we found that 29% of the accessible SVAs and LTR5Hs harboured the full
205 *coordinator motif* sequence, as opposed to only 14% of the non-accessible TEs. This suggests
206 that the human-specific TEs accessible in CNCCs are significantly more enriched for the
207 *coordinator motif* relative to the non-accessible ones (Fisher's Exact Test $p < 0.00001$).
208 In addition, the motifs for other CNCC signature transcription factors, such as AP2α (*TFAP2A*),
209 SOX9/10, SLUG and FOXD3 were also found as significantly enriched (Fig. 2d; Appendix Fig.
210 2d,e; Appendix File S3). Given the prevalence of the *coordinator* motif in accessible LTR5Hs

211 and SVAs, we investigated whether these TEs are directly bound by TWIST1 in human
212 CNCCs. To address this, we leveraged publicly available TWIST1 ChIP-seq data generated
213 in iPSC-derived CNCCs (Kim et al., 2024), which revealed TWIST1 ChIP-seq signal at over
214 half of the accessible LTR5Hs and SVA in human CNCCs (Fig. 2e).
215 Overall, these findings suggest that DNA sequence and transcription factor binding are a major
216 driver for TE co-option as active CNCC enhancers.
217 Finally, we examined whether the LTR5Hs and SVAs accessible in CNCCs integrated into
218 previously existing enhancers or transcriptionally inactive genomic regions. To investigate this,
219 we analyzed regions extending 250 bp upstream and downstream of these accessible TEs,
220 assessing their accessibility in chimpanzee iPSC-derived CNCCs using publicly available
221 paired-end ATAC-seq data (Prescott et al., 2015; Data ref: Prescott et al., 2015). Notably, we
222 observed no accessibility signal in any of these regions (Appendix Fig. S3), suggesting that
223 the hominoid-specific transposons likely established novel cis-regulatory elements rather than
224 integrating into pre-existing active enhancer regions.
225
226 **Repression of LTR5Hs and SVAs impairs expression of CNCC-migration genes**
227 Our experiments so far identified ~550 LTR5Hs and SVAs (half of which human-specific)
228 displaying active enhancer signature in human CNCCs. Since our CRISPRi system enables
229 the simultaneous repression of ~75% of these elements, we next investigated whether their
230 repression had significant effects on the CNCC transcriptome. To this end, we differentiated
231 our doxycycline-treated CRISPRi lines (+ and -gRNAs) into CNCCs and performed RNA-seq.
232 First, we analyzed gene expression in relation to the nearest transcription start sites (TSS) of
233 the 256 accessible human-specific SVAs and LTR5Hs. In total, we identified 107 genes
234 located near these elements that were actively expressed in CNCCs (median TPM >1 across
235 all -gRNA replicates). Overall, the expression of these genes was significantly decreased upon
236 TE repression (Wilcoxon's Rank Sum test $p < 0.037$; Appendix Fig. S4a), with 83/107 (=
237 77.5%) displaying lower expression in the +gRNA sample relative to the -gRNA counterpart
238 (Appendix File S4). Consistent with LTR5Hs playing a prominent role in CNCC, 71 of the 83
239 genes (= 86%) with decreased expression upon CRISPR-i were the nearest gene to an
240 accessible LTRH5s.
241 We leveraged publicly available RNA-seq data from CNCCs derived from chimpanzee iPSCs
242 (Prescott et al., 2015), which we reanalysed using our pipeline, to compare the expression of
243 these 107 genes between the two closely related ape species. This analysis revealed that
244 these genes are typically expressed at significantly higher levels in humans than in
245 chimpanzees (Fig. 3a; Appendix File S4). However, repressing the SVAs and LTR5Hs
246 abolished most of this expression difference between the two species (Fig. 3a), suggesting a
247 direct role for human-specific TEs in species-specific CNCC gene regulation. Consistent with

248 this, repressing the hominoid-specific TEs increased the correlation between human and
249 chimpanzee expression levels for these genes (Appendix Fig. S4b).
250 Next, we examined transcriptome-wide effects. Differential gene expression analysis identified
251 795 genes that were significantly differentially expressed between +gRNA and -gRNA CNCCs
252 (FDR < 0.05; FC < -1.5 or > 1.5; Fig. 3b; Appendix File S5). Of these, 501 genes were
253 downregulated, while 294 genes were upregulated in the +gRNA samples (Fig. 3b). Gene
254 ontology enrichment analysis of the downregulated genes revealed a significant enrichment
255 for cell migration-related processes, suggesting that many of these genes play key roles in
256 CNCC migration (Fig. 3c; Appendix File S6). In line with these findings, gene ontology
257 enrichment analysis performed on the 107 genes expressed genes located near accessible
258 LTR5Hs and human-specific SVAs also identified cell migration as one of the top-5 enriched
259 pathways, despite the small sample size (Appendix File S7). Conversely, upregulated genes
260 were primarily associated with mitochondrial and cell division processes (Appendix File S8).
261 It is worth noting that only 3 of the differentially expressed genes had an intronic SVA or
262 LTR5Hs, suggesting that the high number of differentially expressed genes is not an artifact
263 of CRISPRi mediated repression at gene bodies.
264
265 **Silencing hominoid-specific TEs functionally affects CNCC migratory potential *in vitro***
266 Since cell migration was the predominant signature enriched in the downregulated genes, we
267 investigated whether repressing hominoid-specific SVAs and LTR5Hs could functionally affect
268 CNCC migration. To test this, we performed a transwell migration assay, in which hiPSC-
269 CNCCs were seeded on geltrex-coated transwell membranes overnight and subsequently
270 exposed to medium supplemented with the general chemoattractant fetal bovine serum (FBS)
271 in the lower chamber (Fig. 4a). After 24 hours of incubation, comparison of the –gRNA and
272 +gRNA lines revealed a significant reduction in CNCC migration across the membrane upon
273 repression of hominoid-specific TEs, suggesting impaired migratory capacity (Fig. 4b,c).
274 Additionally, we performed a wound healing assay which showed significantly impaired wound
275 closure of the +gRNA CNCCs compared to -gRNA CNCCs when exposed to medium+10%
276 FBS for 8h (Fig. 4d,e). Altogether, these findings are consistent with the RNA-seq data and
277 suggest that SVAs and LTR5Hs-driven regulatory activity contributes to regulate human CNCC
278 migration.
279
280 **The LTR5Hs and SVAs active in CNCCs are silent in most human cell-types**
281 Finally, we investigated whether the 256 human-specific SVAs and LTR5Hs with active
282 enhancer signature in CNCCs were also showing cis-regulatory signature in other human cell
283 types. To address this, we leveraged publicly available H3K27ac ChIP-seq data from 14 cell
284 types generated by the Roadmap Epigenomics Consortium, including distinct brain regions,

lung, aorta, adipose tissue, pancreas and spleen (Kundaje et al., 2015; Data ref: Kundaje et al., 2015). This analysis revealed that, in addition to CNCCs, these 256 TE exhibit active enhancer signature exclusively in endomesodermal cells, with a subset also active in iPSCs (Fig. 5). In contrast, they remain completely silenced in all other cell types (Fig. 5). The activation of these elements in endomesodermal cells is unsurprising, as a previous study from our lab has shown that human-specific SVAs are highly enriched for the motif of the key mesodermal regulator EOMES (= TBR2; Patoori et al., 2022). Similarly, the co-option of SVAs and LTR5Hs as regulatory elements in human iPSCs and ESCs has been suggested by previous research (Barnada et al., 2022; Fuentes et al., 2018; Pontis et al., 2019).

In summary, these findings support the notion that TE co-option as functional cis-regulatory elements is largely a cell-type-specific process, with distinct subsets of human-specific TEs contributing to regulatory networks in different developmental contexts. However, a more comprehensive analysis of additional cell types should be performed to further support this model.

Discussion

Transposable elements (TEs) have historically been viewed as genomic parasites with little relevance beyond their self-propagation mechanisms. Yet, over the past two decades, numerous studies have shown that TEs can substantially influence gene regulatory architectures, driving lineage-specific developmental programs and morphological variation (Chuong et al., 2017; Feschotte, 2008; Fueyo et al., 2022; Patoori et al., 2022; Sundaram & Wysocka, 2020; Trizzino et al., 2017). In this regard, the vertebrate cranial neural crest cell (CNCC) population, which plays a pivotal role in craniofacial morphogenesis, offers an especially intriguing system for the investigation of TE co-option as a source of regulatory novelty (Bronner & LeDouarin, 2012; Gokhman et al., 2021; Minoux & Rijli, 2010; Prescott et al., 2015). Over the course of vertebrate evolution, craniofacial diversity has been shaped by small but potent modifications in the gene regulatory circuits of the neural crest (Gokhman et al., 2021; Prescott et al., 2015). In this context, our findings suggest that hominoid-specific TEs contribute to these modifications by providing new enhancer platforms that alter CNCC gene expression, pointing to a direct role for TEs in the emergence of human-specific craniofacial features (Gokhman et al., 2021; Prescott et al., 2015).

CNCCs are a multipotent, migratory cell population that emerges from the border region of the neural tube and subsequently disperses into developing craniofacial structures, the peripheral nervous system, and other tissues (Simões-Costa et al., 2015; Theveneau & Mayor, 2012). Understanding how species-specific genomic elements, such as hominoid-specific TEs, modulate CNCC development can shed light on the evolutionary mechanisms underlying morphological divergence, particularly in the craniofacial region (Capra et al., 2013; Prescott

322 et al., 2015). Specifically, in this study we demonstrate that LTR5Hs and SVAs, two families
323 of TEs unique to hominoids, function as enhancers within human CNCCs. Using integrative
324 approaches that combined chromatin accessibility profiling, transcriptomic analysis, and
325 functional perturbation via CRISPR-interference, we reveal that hundreds of these TEs display
326 active enhancer signatures and exert direct regulatory control over genes crucial for CNCC
327 migration. These findings are in line with previous studies showing that TEs can be repurposed
328 as developmental enhancers, thereby contributing to species-specific gene regulatory
329 landscapes in primates (Jacques et al., 2013; Patoori et al., 2022; Trizzino et al., 2017). Our
330 data also implicate these TE-derived enhancers in driving human-specific craniofacial
331 regulatory programs, as evidenced by the fact that repressing LTR5Hs and SVAs reduces the
332 expression of dozens of genes in human CNCCs to levels normally observed in chimpanzees.
333 Notably, LTR5Hs and SVAs have historically been linked to regulatory innovation in primates,
334 though their roles in neural crest biology have remained unexplored (Fuentes et al., 2018;
335 Imbeault et al., 2017; Patoori et al., 2022; Pontis et al., 2019).
336 One of the central questions in evolutionary developmental biology is how minor alterations in
337 deeply conserved developmental pathways can yield significant morphological divergence
338 (Carroll, 2005; King & Wilson, 1975). The CNCC population, which is indispensable for
339 craniofacial bone and cartilage formation, serves as an excellent proof of principle in this
340 regard. It has been suggested that relatively small changes in CNCC gene expression can
341 profoundly impact facial shape and size (Preprint: Khouri-Farah et al., 2025; Le Douarin &
342 Dupin, 2018; Minoux & Rijli, 2010; Preprint: Mitchell et al., 2025; Prescott et al., 2015). Our
343 study extends this framework by proposing that TEs represent a flexible reservoir of regulatory
344 motifs capable of integrating into pre-existing gene regulatory networks, fine-tuning CNCC
345 specification and migration. These findings are consistent with previous reports showing that
346 TEs have been exapted into tissue-specific enhancers in various lineages, including immune
347 cells, brain cell-types, embryonic stem cells, and endometrial tissue (Chuong et al., 2017;
348 Frost et al., 2023; Lynch et al., 2011; Trizzino et al., 2018; J. Wang et al., 2014).
349 Importantly, while most of the LTR5Hs elements are present a “solo LTRs” in the human
350 genome, a few of them, also targeted by our gRNAs, encode full-length proviral sequences
351 that express Rec, Env and Np9 subunits. Previous studies have shown that the Rec and Env
352 subunits can effectively influence cell migration, for instance in melanocytes in melanoma
353 (Singh et al., 2020). Therefore, we cannot rule out that the impairment of CNCC migration is
354 not only due to repression of the LTR5Hs-derived enhancer activity, but also to the repression
355 of the encoded proteins of the full-length proviral sequences.
356 While correlative evidence can implicate TEs as enhancers, functional validation is key to
357 establishing their regulatory impact. By employing a CRISPRi approach that targeted
358 approximately 75% of all the LTR5Hs and SVAs active in CNCCs, we observed pronounced

359 effects on gene expression with a strong enrichment for processes related to cell migration,
360 which is indispensable for CNCCs to navigate into the developing facial primordia (Theveneau
361 & Mayor, 2012). The accessible LTR5Hs and SVAs that remained unaffected by CRISPRi, as
362 they were not targeted by our gRNAs, comprised of only 68 elements. Analysis of the nearest
363 genes associated with these elements did not reveal enrichment for any specific biological
364 pathways. Nevertheless, motif enrichment analysis against scrambled backgrounds identified
365 significant enrichment for binding motifs of key CNCC transcription factors, including TFAP2A,
366 SOX9/10, and TWIST1. These findings suggest that a small subset of TEs potentially bound
367 by NCC transcription factors may escape effective silencing in our experimental system,
368 although they represent a minority of elements.
369 Overall, our results not only reinforce the notion that TEs influence CNCC gene networks but
370 also demonstrate that their regulatory input is significant enough to modulate key
371 developmental pathways. This model agrees with evidence from other contexts in which TEs
372 have driven evolutionary innovations. For instance, MER41 elements in the human genome
373 have been exapted as enhancers regulating immune responses (Chuong et al., 2017).
374 Similarly, in the endometrium and placenta, endogenous retroviral LTRs have been implicated
375 in the evolution of pregnancy-specific gene regulatory networks (Frost et al., 2023; Lynch et
376 al., 2011). Our study adds craniofacial development to the growing list of developmental
377 systems shaped by TE co-option, further highlighting the broad evolutionary relevance of
378 these mobile elements.
379 TE co-option relies on the inherent or mutated presence of transcription factor binding sites
380 within TE sequences (Barnada et al., 2022; Bejerano et al., 2006; Feschotte, 2008; Patoori et
381 al., 2022; Trizzino et al., 2017, 2018). In this study we show that LTR5Hs and SVAs
382 domesticated as enhancers in CNCCs harbour binding sites for the CNCC *coordinator* motif
383 (Kim et al., 2024; Prescott et al., 2015), as well as motifs for TFAP2A, SOX9/10 and other key
384 regulators of neural crest identity. We hypothesize that these factors bind cooperatively to
385 multi-part motifs within the TE loci, enabling the formation of enhancer complexes that drive
386 spatial and temporal gene expression programs in CNCCs. Notably, TFAP2A expression was
387 reduced, albeit modestly, upon TE repression. TFAP2A is critical for CNCC specification and
388 also migration, and it is possible that dysregulation of this factor could, at least in part, underpin
389 some of the aberrant migratory phenotypes.
390 Disruptions to CNCC gene regulatory networks can underlie congenital anomalies such as
391 cleft lip and palate, craniosynostosis, and other craniofacial malformations (Preprint: Khouri-
392 Farah et al., 2025; Trainor, 2010). Given that TE-derived enhancers are integral to the CNCC
393 transcriptional program, mutations or epigenetic dysregulations at these loci could contribute
394 to such disorders. Future studies investigating the links between TE variations and craniofacial
395 pathologies may reveal novel diagnostic markers or therapeutic targets.

In addition, comparative investigations in other hominoids, including gorillas and orangutans, could help unravel whether other TEs have been similarly co-opted in the cranial neural crest. Such research would clarify whether TE-driven craniofacial enhancer innovations are a hallmark across all hominoids or largely unique to the human lineage, shedding light on how small-scale genetic elements can produce macro-evolutionary changes in form and function.

Finally, our study has some limitations. Firstly, employing distinct gRNAs for SVAs and LTRHs would be ideal to more precisely differentiate the roles of these two TE families in CNCC development. Additionally, we assigned genes to TE-derived enhancers based on genomic proximity, but enhancer-promoter contact maps would offer more precise enhancer-gene associations. Unfortunately, genome-wide contact maps are currently unavailable for CNCCs. Relatedly, the expression of a single gene is often regulated by multiple redundant enhancers, complicating the precise determination of individual enhancer contributions without CNCC-specific enhancer-promoter contact data. Consequently, the absence of a detectable gene expression change upon CRISPRi does not necessarily exclude enhancer activity of a specific TE, as compensatory enhancers might mask the loss-of-function phenotype.

Furthermore, while our Gene Ontology analysis robustly highlighted a "cell migration" signature, functionally validated through transwell and wound healing assays, we could not definitively identify the exact genes responsible for the altered migratory phenotype observed upon repression of hominoid-specific TEs.

Another limitation is our reliance on uniquely mapping sequencing reads. Although this approach ensures specificity, it likely omits biologically meaningful signals from multi-mapping reads. Lastly, while we hypothesize that the observed phenotype arises from the co-option of TEs into CNCC migration-associated enhancers, additional validation via techniques like ChIP-STARR-seq combined with targeted genetic perturbations would be help substantiate this model and confirm that disruption of these enhancers directly influences gene expression and related cellular behaviors.

In conclusion, our findings provide further evidence for TEs as highly adaptive genomic elements that actively contribute to shaping developmental and evolutionary trajectories. Through combined roles in CNCC specification, migration, and potentially other lineage-specific developmental programs, TEs demonstrate how evolutionary tinkering at the regulatory level can yield morphological diversity.

Materials and Methods

Generation of doxycycline-inducible dCas9-KRAB hiPSC lines

A plasmid containing a tetracycline-inducible dCas9-KRAB expression cassette flanked by piggyBac recombination sites was obtained from the Wysocka Lab at Stanford University. This plasmid, referred to as 'p-dCas9-KRAB,' provides constitutive puromycin resistance, enabling selection of stable clones when co-expressed with the piggyBac transposase plasmid ('p-PB-Transposase,' Systems Bioscience). For the -gRNAs line, the C2277 hiPSC line was co-transfected with p-dCas9-KRAB and p-PB-Transposase by Applied StemCell Inc. (C2277-A, -gRNAs line). Next, a piggyBac transposon plasmid ('p-sgRNA,' Systems Bioscience) containing two sgRNAs targetting ~80% of annotated SVAs and LTR5Hs in humans was obtained based on a previously published study(Pontis et al., 2019). This plasmid confers constitutive dual sgRNA expression and geneticin resistance. For the +gRNAs line, the C2277 hiPSC line was co-transfected with p-dCas9-KRAB, p-PB-Transposase, and p-sgRNA (C2277-B, +gRNA line). Puromycin (0.125 µg/mL) only (-gRNAs line) or puromycin (0.125 µg/mL) and geneticin (100 µg/mL) (+gRNAs line) were introduced for multiple days to obtain purified colonies. Both cell lines were authenticated by STR profiling and screened for mycoplasma contamination prior to receival.

iPSC culture and NCC differentiation

Human iPSC lines C2277-A (-gRNAs) and C2277-B (+gRNAs) were cultured in feeder-free, serum-free 2D culture at 37°C and 5% CO_2. For the generation of NCCs, the differentiation method was derived from the protocol published by Leung et al. (2016). Briefly, hiPSCs were grown in mTeSR Plus (StemCell Technologies, 100-0276) on Geltrex-coated (Thermofisher, A1413302) 6-well plates until reaching ~80% confluency. Differentiation was initiated by plating $2x10^6$ hiPSCs in Neural Crest Differentiation media (DMEM/F12 (Gibco, A4192002), 2% B-27 supplement (Fisher Scientific, 15717988), 3 µM CHIR99021 (Stratech, S1263-SEL-5mg), 0.5% bovine serum albumin (Fisher Scientific, 12881630), 1X glutaMAX supplement (Gibco, 35050061), 1% penicillin-streptomycin (Gibco, 15070063)) onto Geltrex-coated 6-well plates supplemented with 10 µM Y-27632 (Cambridge Bioscience, HY-119937-5MG). The following days daily media changes were performed and 2 µg/mL doxycycline was added to the culture media from day 2 onwards (i.e. 24h after the start of differentiation). NCC differentiation was assessed after 5 days.

Immunocytochemistry

HiPSCs-NCCs were harvested by incubation with StemPro Accutase (Gibco, A1110501) for 5-10 min followed by aspiration and detachment with DMEM/F12, and subsequently seeded

468 onto 16 mm coverslips in 12-well plates coated with Geltrex and left overnight to attach before
469 fixation with 4% paraformaldehyde/PBS for 15 min at 37°C. After washing with PBS, the fixed
470 cells were stored in PBS until staining. HiPSC-NCCs were subsequently permeabilised with
471 0.1% Triton-X-100/PBS (Merck, 648463) for 10 min at RT and blocked using 10% donkey
472 serum/PBS (Abcam, AB7475) for 1h at RT. Cells were stained with primary antibodies
473 overnight at 4°C in the dark, washed and stained with secondary antibodies for 30 min at 37°C.
474 The antibodies used can be found in Reagents and Tools Table. After a subsequent washing
475 step, cells were counterstained with 1 µg/mL DAPI (BioLegend, 422801). Washing steps were
476 performed with 0.1% Tween:PBS (Promega, H5152). Images were acquired using a Zeiss
477 Axio Observer and further processing was done using ImageJ. Normalised intensity was
478 calculated by dividing the signal intensity of each frame by the number of cells.
479
480 **Western blot**
481 Cells were lysed in radioimmunoprecipitation assay (RIPA) buffer (Fisher Scientific, 10230544)
482 supplemented with a Pierce protease inhibitor tablet (Fisher Scientific, 15614189). The lysates
483 were vortexed for 30 s and incubated on ice for 30 min. Samples were then centrifuged at
484 17,000 g for 10 min at 4°C, and the supernatant was collected. Protein concentration was
485 determined using a Pierce BCA Protein Assay Kit (Fisher Scientific, 23225) according to the
486 manufacturer's protocol. The plate was incubated at 37°C for 30 min and analyzed using the
487 SpectraMax M2 microplate reader (Molecular Devices) at 562 nm. 10 ug of protein were
488 denatured in Laemmli Buffer (Fisher Scientific, J61337.AC) at 95°C for 5 min. Proteins were
489 separated using a 4–12% Novex Tris-Glycine Mini Protein Gel (Invitrogen, XP04122BOX) in
490 Novex Tris-Glycine SDS Running Buffer (Fisher Scientific, 11559066) for 90 min. Proteins
491 were transferred onto a nitrocellulose membrane using the Mini Trans-Blot Cell system with
492 NuPAGE Transfer Buffer (Life Technologies, NP00061) for 1h. Membranes were blocked in
493 Li-Cor Intercept Blocking Buffer (Li-Cor, 927-70001) for 1h at RT, then incubated overnight at
494 4°C with primary antibodies (see Reagents and Tools Table) diluted in Intercept Blocking
495 Buffer with 0.2% Tween. The following day, washes were performed in 0.1% Tween/PBS and
496 membranes were incubated with secondary antibodies (see Reagents and Tools Table) for 30
497 min before imaging on a LiCor Odyssey XF imaging system.
498
499 **Real-time qPCR**
500 Total RNA was isolated using the Monarch Total RNA miniprep kit (New England BioLabs,
501 T2010) following the manufacturer's instructions. Briefly, harvested cells were lysed in RLT
502 buffer. The lysate was then passed through a gDNA column and centrifuged at 16,000 g for 1
503 min. Next, 70% ethanol was added to the lysate, which was transferred to an RNeasy silica
504 column and centrifuged at 16,000 g for 1 min. The column was washed followed by DNase I

505 treatment for 15 min at RT. Additional wash steps were performed followed by a final dry
506 centrifugation at 12,000 rpm for 1 minute. RNA was eluted in RNase-free ddH_2O, and
507 centrifuged at 16,000 g for 1 min. The eluted RNA was either used immediately or stored at -
508 80°C. Reverse transcription into cDNA was performed using the Maxima First Strand cDNA
509 Synthesis kit with the following thermal cycler settings: 10 min at 25°C, 15 min at 50°C, and 5
510 min at 85°C. Gene expression was quantified via real-time PCR PowerUp SYBR Green
511 Supermix (Life Technologies, A46112). Primers for each gene are listed in the Reagents and
512 Tools Table. GAPDH was used as housekeeping gene. RT-qPCR was performed using a CFX
513 Connect Real-Time PCR Detection System (Bio-rad) with the following cycling parameters: 5
514 min at 95°C, 40 cycles of 15 s at 95°C, 30 s at 60°C, and 30 s at 72°C.
515
516 **Transwell migration assay**
517 24-well inserts (8 µM, Starstedt) were coated on both sides with ~22 µg/cm² Geltrex for 1 h at
518 37°C. After removing excess liquid, 1 × 10^5 hiPSC-NCCs were seeded in Neural Crest
519 Differentiation media + 10 µM Y-27632 in the upper compartment and incubated overnight for
520 attachment. The following day, the media was replaced and Neural Crest Differentiation media
521 supplemented with 10% FBS was added to the lower compartment. Migration was assessed
522 by fixing the membranes in 4% paraformaldehyde/PBS for 15 min at RT, followed by PBS
523 washing and DAPI staining for 15 min at RT. To ensure visualization of migrated cells only, the
524 upper surface of the insert was carefully swabbed with a cotton swab before fixation.
525 Membranes were then excised and mounted on microscope slides for imaging. 10X images
526 were captured from four different fields of view, and the average number of migrated cells was
527 counted. Images were acquired using a Zeiss Axio Observer and migration was quantified
528 using ImageJ.
529
530 **Wound healing assay**
531 HiPSC-NCCs were seeded into 24-well plates at a density of 2.5 x10^5 cells/cm^2 overnight to
532 generate confluent monolayers. A scratch wound was made with a P200 tip and following a
533 wash with PBS, hiPSC-NCCs were incubated with Neural Crest Differentiation media + 10%
534 FBS. After 8h, migration was assessed and the wounds were imaged EVOS XL Core Cell
535 Imaging System. Wound closure was measured automatically using an ImageJ plugin
536 (Suarez-Arnedo et al., 2020).
537
538 **Bulk RNA-seq library preparation**
539 Total RNA was isolated using the Monarch Total RNA miniprep kit (New England BioLabs,
540 T2010) following the manufacturer's instructions. RNA was quantified using a Nanodrop
541 spectrophotometer and RNA integrity was checked on a Tapestation 2200 (Agilent). Only

542 samples with a RIN > 7.0 were used for transcriptome analysis. RNA libraries were prepared
543 using 300 ng of total RNA input using the NEBNext Poly(A) mRNA Magnetic Isolation
544 Module(E7490) and NEBNext® Ultra II Directional RNA Library Prep Kit for Illumina (E7760)
545 according to the manufacturer's instructions. PE150 sequencing was performed on a
546 NovaSeq X Plus instrument (Illumina).
547
548 **RNA-seq analysis**
549 Adapters were removed using TrimGalore!, and gene-level read counts were obtained with
550 Kallisto (Bray et al., 2016). Differential gene expression analysis was performed using DESeq2
551 (Love et al., 2014). GO enrichment analysis was performed using Webgestalt 2019 (Liao et
552 al., 2019). TE expression analysis was performed using TEtranscripts (Jin et al., 2015).
553 Additional statistical analysis was carried out using R (version 4.2.2) and GraphPad Prism 10.
554
555 **ChIP-seq library preparation**
556 10 million hiPSC-NCCs were crosslinked in 1% paraformaldehyde for 5 min at RT with mild
557 rotation. Crosslinking was quenched with 0.125M glycine by rotation for 5 min at RT. Cells
558 were washed twice with cold PBS and were snap-frozen for 15 min on dry ice. Samples were
559 stored at -80 °C until further processing. Cells were resuspended in 1 mL ChIP buffer (150
560 mM NaCl, 1% Triton X-100, 500 mM DTT, 10 mM Tris-HCl, 5 mM EDTA) supplemented with
561 Pierce protease inhibitor tablet and incubated on ice for 10 min. SDS was added to each
562 sample to a final concentration of 0.3%, and chromatin was sheared using the following
563 settings: 9 min, duty factor 5%, 6°C in a Covaris M220 Focused-Ultrasonicator. Chromatin
564 fragment size was assessed on a Tapestation 2200.
565 The chromatin lysates were then centrifuged at 13,000 g for 10 min at 4 °C and supernatant
566 was subsequently incubated with ChIP buffer supplemented with Pierce protease inhibitor and
567 Dynabeads Protein G magnetic beads (Invitrogen) along with 3 µg of H3K9me3 antibody
568 (Abcam, ab8898) and incubated overnight at 4 °C under mild rotation. The following day,
569 samples were placed in a magnetic rack and washed twice with Mixed Micelle Wash Buffer
570 (150 mM NaCl, 1% Triton X-100, 0.2% SDS, 20 mM Tris-HCl, 5 mM EDTA, 65% sucrose),
571 twice with Buffer 200 (200 mM NaCl, 1% Triton X-100, 0.1% sodium deoxycholate, 25 mM
572 HEPES, 10 mM Tris-HCl, 1 mM EDTA), twice with LiCl/detergent wash (250 mM LiCl, 0.5%
573 sodium deoxycholate, 0.5% NP-40, 10 mM Tris-HCl, 1 mM EDTA), once with cold TE. The
574 beads were resuspended in TE + 1% SDS and incubated at 65 °C for 10 min at 1200 rpm to
575 elute immunocomplexes. The elution was repeated twice and the samples were incubated
576 overnight at 65˚C to reverse cross-linking. The following day, Proteinase K (0.5 mg/mL) was
577 added to digest samples at 65 °C for 1h. DNA was purified using the Zymo ChIP DNA Clean
578 and Concentrator kit (Zymo, D5205) and quantified with the Quantifluor ONE dsDNA system

(Promega, E4871). DNA libraries were prepared using the NEBNext Ultra II DNA library Prep Kit (E7645L) for Illumina. PE150 sequencing was performed on a NovaSeq X Plus instrument (Illumina).

ChIP-seq analysis

Adapters were removed with TrimGalore! and reads were aligned to hg38 using Burrows-Wheeler Alignment tool, with the MEM algorithm (Li & Durbin, 2009). Uniquely mapping reads were filtered (MAPQ>10) and PCR duplicates were removed and mitochondrial reads were discarded. Peaks were called using HOMER with default parameters at 5% FDR (Heinz et al., 2010). All statistical analyses were performed using BEDTools (Quinlan & Hall, 2010), deepTools (Ramírez et al., 2014), R (version 4.2.2) and GraphPad Prism 10.

ATAC-seq library preparation

DNA libraries were prepared following the ATAC-Seq kit (Active Motif, 53150) according to the manufacturer's instructions. 100,000 cells were tagmented per sample, DNA was purified using SPRI beads and amplified with dual index primers. Libraries were assessed for size distribution using the TapeStation 2200 and PE150 sequencing was performed on a NovaSeq X Plus instrument (Illumina).

ATAC-seq analysis

Adapters were removed with TrimGalore! and reads were aligned to hg38 using Burrows-Wheeler Alignment tool, with the MEM algorithm (Li & Durbin, 2009). With SAMTools (Li et al., 2009), uniquely mapping reads were filtered (MAPQ>10), PCR duplicates were removed and mitochondrial reads were discarded. Consensus peaks were determined in each cell line using BEDTools (Quinlan & Hall, 2010). Motif analysis was performed using HOMER (Heinz et al., 2010). All further downstream analysis was performed using BEDTools and deepTools (Ramírez et al., 2014).

Statistics

RT-qPCR, transwell migration and image quantification data were analysed using Graphpad Prism 10 software (Graphpad, San Diego, CA). Data is represented as mean ± standard error of mean (SEM). Statistical significance was accepted at $p < 0.05$. Sample sizes were not determined using statistical methods but were based on previous experiments under similar conditions. Blinding was not performed on experiments but data analysis was automated for all experiments (e.g. intensity tresholds or automated plugins in FIJI). Sequencing data was analysed using BEDTools, DeepTools, and R as indicated. Motif analysis was performed using HOMER. GO enrichment analysis was performed using Webgestalt 2019.

Acknowledgements

The authors thank the Wysocka group at Stanford (and particularly Dr. Raquel Fueyo) for providing the dCAS9-KRAB vector, and Andrew Isopi and Dr. Samantha Barnada (Thomas Jefferson University), for designing the plasmid with the sg-RNAs. We thank the Facility for Imaging by Light Microscopy (FILM) at Imperial College London for providing access to instrumentation and technical support, which is part-supported by funding from the Wellcome Trust (grant 104931/Z/14/Z) and BBSRC (grant BB/L015129/1). For this work, MT was funded by Biotechnology and Biological Sciences Research Council (BBSRC, grant BB/Y000854/1).

Data availability

RNA-seq, ATAC-seq, and ChIP-seq data have been deposited in the Gene Expression Omnibus (GEO) under accession code GEO: GSE292478. (https://www.ncbi.nlm.nih.gov/geo/query/acc.cgi?acc=GSE292478) and are publicly available as of the date of manuscript submission.

Disclosure and competing interest statement

The authors declare no competing interests.

Author contributions

MT and LD designed the project. LD performed most of the experiments. ZHM, MD and BGDV contributed to some of the experiments. LD, MT, and AK analyzed the data. LD and MT and wrote the manuscript. All the authors read and approved the manuscript.

References

Ahlstrom, J. D., & Erickson, C. A. (2009). The neural crest epithelial-mesenchymal transition in 4D: A 'tail' of multiple non-obligatory cellular mechanisms. *Development*, *136*(11), 1801–1812. https://doi.org/10.1242/dev.034785

Bajpai, R., Chen, D. A., Rada-Iglesias, A., Zhang, J., Xiong, Y., Helms, J., Chang, C. P., Zhao, Y., Swigut, T., & Wysocka, J. (2010). CHD7 cooperates with PBAF to control multipotent neural crest formation. *Nature*, *463*(7283), 958–962. https://doi.org/10.1038/nature08733

Barnada, S. M., Giner de Gracia, A., Morenilla-Palao, C., López-Cascales, M. T., Scopa, C., Waltrich, F. J., Mikkers, H. M. M., Cicardi, M. E., Karlin, J., Trotti, D., Peterson, K. A., Brugmann, S. A., Santen, G. W. E., McMahon, S. B., Herrera, E., & Trizzino, M. (2024). ARID1A-BAF coordinates ZIC2 genomic occupancy for epithelial-to-mesenchymal transition in cranial neural crest specification. *The American Journal of Human Genetics*. https://doi.org/10.1016/j.ajhg.2024.07.022

Barnada, S. M., Giner de Gracia, A., Morenilla-Palao, C., López-Cascales, M. T., Scopa, C., Waltrich, F. J., Mikkers, H. M. M., Cicardi, M. E., Karlin, J., Trotti, D., Peterson, K. A., Brugmann, S. A., Santen, G. W. E., McMahon, S. B., Herrera, E., & Trizzino, M. (2024). Gene Expression Omnibus GSE261846 (https://www.ncbi.nlm.nih.gov/geo/query/acc.cgi?acc=GSE261846). [DATASET]

Barnada, S. M., Isopi, A., Tejada-Martinez, D., Goubert, C., Patoori, S., Pagliaroli, L., Tracewell, M., & Trizzino, M. (2022). Genomic features underlie the co-option of SVA transposons as cis-regulatory elements in human pluripotent stem cells. *PLoS Genetics*, *18*(6), 1–19. https://doi.org/10.1371/journal.pgen.1010225

Bejerano, G., Lowe, C. B., Ahituv, N., King, B., Siepel, A., Salama, S. R., Rubin, E. M., Kent, W. J., & Haussler, D. (2006). A distal enhancer and an ultraconserved exon are derived from a novel retroposon. *Nature*, *441*(1), 87–90. https://doi.org/10.1038/nature04696

Bourque, G., Leong, B., Vega, V. B., Chen, X., Yen, L. L., Srinivasan, K. G., Chew, J. L., Ruan, Y., Wei, C. L., Huck, H. N., & Liu, E. T. (2008). Evolution of the mammalian transcription factor binding repertoire via transposable elements. *Genome Research*, *18*(11), 1752–1762. https://doi.org/10.1101/gr.080663.108

Bray, N. L., Pimentel, H., Melsted, P., & Pachter, L. (2016). Near-optimal probabilistic RNA-seq quantification. *Nature Biotechnology*, *34*(5), 525–527. https://doi.org/10.1038/nbt.3519

Bronner, M. E., & LeDouarin, N. M. (2012). Development and evolution of the neural crest: An overview. In *Developmental Biology* (Vol. 366, Issue 1, pp. 2–9). Academic Press Inc. https://doi.org/10.1016/j.ydbio.2011.12.042

Capra, J. A., Hubisz, M. J., Kostka, D., Pollard, K. S., & Siepel, A. (2013). A Model-Based Analysis of GC-Biased Gene Conversion in the Human and Chimpanzee Genomes. *PLoS Genetics*, *9*(8). https://doi.org/10.1371/journal.pgen.1003684

Carroll, S. B. (2005). Evolution at two levels: On genes and form. In *PLoS Biology* (Vol. 3, Issue 7, pp. 1159–1166). Public Library of Science. https://doi.org/10.1371/journal.pbio.0030245

Chuong, E. B., Elde, N. C., & Feschotte, C. (2016). Regulatory evolution of innate immunity through co-option of endogenous retroviruses. *Science*, *351*(6277), 1083–1087. https://doi.org/10.1126/science.aad5497

Chuong, E. B., Elde, N. C., & Feschotte, C. (2017). Regulatory activities of transposable elements: From conflicts to benefits. In *Nature Reviews Genetics* (Vol. 18, Issue 2, pp. 71–86). Nature Publishing Group. https://doi.org/10.1038/nrg.2016.139

Chuong, E. B., Rumi, M. A. K., Soares, M. J., & Baker, J. C. (2013). Endogenous retroviruses function as species-specific enhancer elements in the placenta. *Nature Genetics*, *45*(3), 325–329. https://doi.org/10.1038/ng.2553

Cordero, D. R., Brugmann, S., Chu, Y., Bajpai, R., Jame, M., & Helms, J. A. (2011). Cranial neural crest cells on the move: Their roles in craniofacial development. *American Journal of Medical Genetics, Part A*, *155*(2), 270–279. https://doi.org/10.1002/ajmg.a.33702

Cosby, R. L., Judd, J., Zhang, R., Zhong, A., Garry, N., Pritham, E. J., & Feschotte, C. (2021). Recurrent evolution of vertebrate transcription factors by transposase capture. *Science*, *371*(6531). https://doi.org/10.1126/science.abc6405

Feschotte, C. (2008). Transposable elements and the evolution of regulatory networks. *Nature Genetics*, *9*, 397–405.

Frost, J. M., Amante, S. M., Okae, H., Jones, E. M., Ashley, B., Lewis, R. M., Cleal, J. K., Caley, M. P., Arima, T., Maffucci, T., & Branco, M. R. (2023). Regulation of

human trophoblast gene expression by endogenous retroviruses. *Nature Structural and Molecular Biology*, *30*(4), 527–538. https://doi.org/10.1038/s41594-023-00960-6

Fuentes, D., Swigut, T., & Wysocka, J. (2018). Systematic perturbation of retroviral LTRs reveals widespread long-range effects on human gene regulation. *ELife*. https://doi.org/10.7554/eLife.35989.001

Fueyo, R., Judd, J., Feschotte, C., & Wysocka, J. (2022). Roles of transposable elements in the regulation of mammalian transcription. *Nature Reviews Molecular Cell Biology*, *23*(7), 481–497. https://doi.org/10.1038/s41580-022-00457-y

Gans, C., & Northcutt, R. G. (1983). Neural Crest and the Origin of Vertebrates: A New Head. *Science*, *220*(4594), 268–273. https://doi.org/10.1126/science.220.4594.268

Gokhman, D., Agoglia, R. M., Kinnebrew, M., Gordon, W., Sun, D., Bajpai, V. K., Naqvi, S., Chen, C., Chan, A., Chen, C., Petrov, D. A., Ahituv, N., Zhang, H., Mishina, Y., Wysocka, J., Rohatgi, R., & Fraser, H. B. (2021). Human–chimpanzee fused cells reveal cis-regulatory divergence underlying skeletal evolution. *Nature Genetics*, *53*(4), 467–476. https://doi.org/10.1038/s41588-021-00804-3

Goubert, C., Zevallos, N. A., & Feschotte, C. (2020). Contribution of unfixed transposable element insertions to human regulatory variation. *Philosophical Transactions of the Royal Society B: Biological Sciences*, *375*(1795). https://doi.org/10.1098/rstb.2019.0331

Heinz, S., Benner, C., Spann, N., Bertolino, E., Lin, Y. C., Laslo, P., Cheng, J. X., Murre, C., Singh, H., & Glass, C. K. (2010). Simple Combinations of Lineage-Determining Transcription Factors Prime cis-Regulatory Elements Required for Macrophage and B Cell Identities. *Molecular Cell*, *38*(4), 576–589. https://doi.org/10.1016/j.molcel.2010.05.004

Imbeault, M., Helleboid, P. Y., & Trono, D. (2017). KRAB zinc-finger proteins contribute to the evolution of gene regulatory networks. *Nature*, *543*(7646), 550–554. https://doi.org/10.1038/nature21683

Jacques, P. É., Jeyakani, J., & Bourque, G. (2013). The Majority of Primate-Specific Regulatory Sequences Are Derived from Transposable Elements. *PLoS Genetics*, *9*(5). https://doi.org/10.1371/journal.pgen.1003504

Jheon, A. H., & Schneider, R. A. (2009). The cells that fill the bill: Neural crest and the evolution of craniofacial development. In *Journal of Dental Research* (Vol. 88, Issue 1, pp. 12–21). https://doi.org/10.1177/0022034508327757

Jin Y, Tam OH, Paniagua E, Hammell M. (2015) TEtranscripts: a package for including transposable elements in differential expression analysis of RNA-seq datasets. *Bioinformatics*. 31(22):3593-9.

Khouri-Farah, N., Winchester, E. W., Schilder, B. M., Robinson, K., Curtis, S. W., Skene, N. G., Leslie-Clarkson, E. J., & Cotney, J. (2025). Gene expression patterns of the developing human face at single cell resolution reveal cell type contributions to normal facial variation and disease risk. *bioRxiv*. https://doi.org/10.1101/2025.01.18.633396

Kim, S., Morgunova, E., Naqvi, S., Goovaerts, S., Bader, M., Koska, M., Popov, A., Luong, C., Pogson, A., Swigut, T., Claes, P., Taipale, J., & Wysocka, J. (2024). DNA-guided transcription factor cooperativity shapes face and limb mesenchyme. *Cell*. https://doi.org/10.1016/j.cell.2023.12.032

Kim, S., Morgunova, E., Naqvi, S., Goovaerts, S., Bader, M., Koska, M., Popov, A., Luong, C., Pogson, A., Swigut, T., Claes, P., Taipale, J., & Wysocka, J. (2024). Gene Expression Omnibus GSE230319 (https://www.ncbi.nlm.nih.gov/geo/query/acc.cgi?acc=GSE230319) [DATASET]

King, M.-C., & Wilson, A. C. (1975). Evolution at Two Levels in Humans and Chimpanzees. *Science*, *188*, 107–116. https://www.science.org

Kunarso, G., Chia, N. Y., Jeyakani, J., Hwang, C., Lu, X., Chan, Y. S., Ng, H. H., & Bourque, G. (2010). Transposable elements have rewired the core regulatory network of human embryonic stem cells. *Nature Genetics*, *42*(7), 631–634. https://doi.org/10.1038/ng.600

Le Douarin, N. M., & Dupin, E. (2018). The “beginnings” of the neural crest. In *Developmental Biology* (Vol. 444, pp. S3–S13). Elsevier Inc. https://doi.org/10.1016/j.ydbio.2018.07.019

Leung, A. W., Leung, A. W., Murdoch, B., Salem, A. F., Prasad, M. S., Gomez, G. A., & García-Castro, M. I. (2016). WNT/β-catenin signaling mediates human neural crest induction via a pre-neural border intermediate. *Development (Cambridge)*, *143*(3), 398–410. https://doi.org/10.1242/dev.130849

Li, H., & Durbin, R. (2009). Fast and accurate short read alignment with Burrows-Wheeler transform. *Bioinformatics*, *25*(14), 1754–1760. https://doi.org/10.1093/bioinformatics/btp324

Li, H., Handsaker, B., Wysoker, A., Fennell, T., Ruan, J., Homer, N., Marth, G., Abecasis, G., & Durbin, R. (2009). The Sequence Alignment/Map format and SAMtools. *Bioinformatics*, *25*(16), 2078–2079. https://doi.org/10.1093/bioinformatics/btp352

Liao, Y., Wang, J., Jaehnig, E. J., Shi, Z., & Zhang, B. (2019). WebGestalt 2019: gene set analysis toolkit with revamped UIs and APIs. *Nucleic Acids Research*, *47*(W1), W199–W205. https://doi.org/10.1093/nar/gkz401

Lieberman, D. E. (1998). Sphenoid shortening and the evolution of modern human cranial shape. *Nature*, *393*(6681), 158–162. https://doi.org/10.1038/30227

Love, M. I., Huber, W., & Anders, S. (2014). Moderated estimation of fold change and dispersion for RNA-seq data with DESeq2. *Genome Biology*, *15*(12). https://doi.org/10.1186/s13059-014-0550-8

Lynch, V. J., Leclerc, R. D., May, G., & Wagner, G. P. (2011). Transposon-mediated rewiring of gene regulatory networks contributed to the evolution of pregnancy in mammals. *Nature Genetics*, *43*(11), 1154–1159. https://doi.org/10.1038/ng.917

Martik, M. L., & Bronner, M. E. (2021). Riding the crest to get a head: neural crest evolution in vertebrates. In *Nature Reviews Neuroscience* (Vol. 22, Issue 10, pp. 616–626). Nature Research. https://doi.org/10.1038/s41583-021-00503-2

Minoux, M., & Rijli, F. M. (2010). Molecular mechanisms of cranial neural crest cell migration and patterning in craniofacial development. In *Development* (Vol. 137, Issue 16, pp. 2605–2621). https://doi.org/10.1242/dev.040048

Mitchell, Z. H., den Hoed, J., Claassen, W., Demurtas, M., Deelen, L., Campeau, P. M., Liu, K., Fisher, S. E., & Trizzino, M. (2025). CHD3 regulates BMP signalling response during cranial neural crest cell specification. *bioRxiv*. https://doi.org/10.1101/2025.02.14.638260

Ostertag, E. M., Goodier, J. L., Zhang, Y., & Kazazian, H. H. (2003). SVA Elements Are Nonautonomous Retrotransposons that Cause Disease in Humans. In *Am. J. Hum. Genet* (Vol. 73).

Pagliaroli, L., Porazzi, P., Curtis, A. T., Scopa, C., Mikkers, H. M. M., Freund, C., Daxinger, L., Deliard, S., Welsh, S. A., Offley, S., Ott, C. A., Calabretta, B.,

Brugmann, S. A., Santen, G. W. E., & Trizzino, M. (2021). Inability to switch from ARID1A-BAF to ARID1B-BAF impairs exit from pluripotency and commitment towards neural crest formation in ARID1B-related neurodevelopmental disorders. *Nature Communications*, *12*(1). https://doi.org/10.1038/s41467-021-26810-x

Patoori, S., Barnada, S. M., Large, C., Murray, J. I., & Trizzino, M. (2022). Young transposable elements rewired gene regulatory networks in human and chimpanzee hippocampal intermediate progenitors. *Development (Cambridge)*, *49*(23). https://doi.org/10.1242/dev.200413

Playfoot, C. J., Duc, J., Sheppard, S., Dind, S., Coudray, A., Planet, E., & Trono, D. (2021). Transposable elements and their KZFP controllers are drivers of transcriptional innovation in the developing human brain. *Genome Research*, *31*(9), 1531–1545. https://doi.org/10.1101/gr.275133.120

Pontis, J., Planet, E., Offner, S., Turelli, P., Duc, J., Coudray, A., Theunissen, T. W., Jaenisch, R., & Trono, D. (2019). Hominoid-Specific Transposable Elements and KZFPs Facilitate Human Embryonic Genome Activation and Control Transcription in Naive Human ESCs. *Cell Stem Cell*, *24*(5), 724-735.e5. https://doi.org/10.1016/j.stem.2019.03.012

Prescott, S. L., Srinivasan, R., Marchetto, M. C., Grishina, I., Narvaiza, I., Selleri, L., Gage, F. H., Swigut, T., & Wysocka, J. (2015). Enhancer Divergence and cis-Regulatory Evolution in the Human and Chimp Neural Crest. *Cell*, *163*(1), 68–83. https://doi.org/10.1016/j.cell.2015.08.036

Prescott, S. L., Srinivasan, R., Marchetto, M. C., Grishina, I., Narvaiza, I., Selleri, L., Gage, F. H., Swigut, T., & Wysocka, J. (2015). Gene Expression Omnibus GSE70751 (https://www.ncbi.nlm.nih.gov/geo/query/acc.cgi?acc=GSE70751) [DATASET]

Quinlan, A. R., & Hall, I. M. (2010). BEDTools: A flexible suite of utilities for comparing genomic features. *Bioinformatics*, *26*(6), 841–842. https://doi.org/10.1093/bioinformatics/btq033

Quinn, J. P., & Bubb, V. J. (2014). SVA retrotransposons as modulators of gene expression. *Mobile Genetic Elements*, *4*(4), e32102. https://doi.org/10.4161/mge.32102

Ramírez, F., Dündar, F., Diehl, S., Grüning, B. A., & Manke, T. (2014). DeepTools: A flexible platform for exploring deep-sequencing data. *Nucleic Acids Research*, *42*(W1). https://doi.org/10.1093/nar/gku365

Roadmap Epigenomics Consortium, Kundaje, A., Meuleman, W., Ernst, J., Bilenky, M., Yen, A., Heravi-Moussavi, A., Kheradpour, P., Zhang, Z., Wang, J., Ziller, M. J., Amin, V., Whitaker, J. W., Schultz, M. D., Ward, L. D., Sarkar, A., Quon, G., Sandstrom, R. S., Eaton, M. L., … Kellis, M. (2015). Integrative analysis of 111 reference human epigenomes. *Nature*, *518*(7539), 317–329. https://doi.org/10.1038/nature14248

Roadmap Epigenomics Consortium, Kundaje, A., Meuleman, W., Ernst, J., Bilenky, M., Yen, A., Heravi-Moussavi, A., Kheradpour, P., Zhang, Z., Wang, J., Ziller, M. J., Amin, V., Whitaker, J. W., Schultz, M. D., Ward, L. D., Sarkar, A., Quon, G., Sandstrom, R. S., Eaton, M. L., … Kellis, M. (2015). Gene Expression Omnibus GSE16256 (https://www.ncbi.nlm.nih.gov/geo/query/acc.cgi?acc=GSE16256) [DATASET]

Sambataro, S., Fiorillo, L., Bocchieri, S., Stumpo, C., Cervino, G., Herford, A. S., & Cicciù, M. (2022). Craniofacial Evolution: From Australopithecus to Modern Man.

Journal of Craniofacial Surgery, *33*(1), 325–332. https://doi.org/10.1097/SCS.0000000000007841

Schmidt, D., Schwalie, P. C., Wilson, M. D., Ballester, B., Gonalves, Â., Kutter, C., Brown, G. D., Marshall, A., Flicek, P., & Odom, D. T. (2012). Waves of retrotransposon expansion remodel genome organization and CTCF binding in multiple mammalian lineages. *Cell*, *148*(1–2), 335–348. https://doi.org/10.1016/j.cell.2011.11.058

Simões-Costa, M., Stone, M., & Bronner, M. E. (2015). Axud1 Integrates Wnt Signaling and Transcriptional Inputs to Drive Neural Crest Formation. *Developmental Cell*, *34*(5), 544–554. https://doi.org/10.1016/j.devcel.2015.06.024

Singh, M., Cai, H., Bunse, M., Feschotte, C., & Izsvák, Z. (2020). Human endogenous retrovirus k rec forms a regulatory loop with mitf that opposes the progression of melanoma to an invasive stage. *Viruses*, *12*(11). https://doi.org/10.3390/v12111303

Spoor, F., Wood, B., & Zonneveld, F. (1994). Implications of early hominid labyrinthine morphology for evolution of human bipedal locomotion. *Nature*, *369*(6482), 645–648. https://doi.org/10.1038/369645a0

Suarez-Arnedo, A., Figueroa, F. T., Clavijo, C., Arbeláez, P., Cruz, J. C., & Muñoz-Camargo, C. (2020). An image J plugin for the high throughput image analysis of in vitro scratch wound healing assays. *PLoS ONE*, *15*(7 July). https://doi.org/10.1371/journal.pone.0232565

Sundaram, V., Cheng, Y., Ma, Z., Li, D., Xing, X., Edge, P., Snyder, M. P., & Wang, T. (2014). Widespread contribution of transposable elements to the innovation of gene regulatory networks. *Genome Research*, *24*(12), 1963–1976. https://doi.org/10.1101/gr.168872.113

Sundaram, V., & Wysocka, J. (2020). Transposable elements as a potent source of diverse cis-regulatory sequences in mammalian genomes. In *Philosophical Transactions of the Royal Society B: Biological Sciences* (Vol. 375, Issue 1795). Royal Society Publishing. https://doi.org/10.1098/rstb.2019.0347

Theveneau, E., & Mayor, R. (2012). Neural crest migration: interplay between chemorepellents, chemoattractants, contact inhibition, epithelial–mesenchymal transition, and collective cell migration. *WIREs Developmental Biology*, *1*(3), 435–445. https://doi.org/10.1002/wdev.28

Trainor, P. A. (2010). Craniofacial birth defects: The role of neural crest cells in the etiology and pathogenesis of Treacher Collins syndrome and the potential for prevention. In *American Journal of Medical Genetics, Part A: Vol. 152 A* (Issue 12, pp. 2984–2994). https://doi.org/10.1002/ajmg.a.33454

Trizzino, M., Kapusta, A., & Brown, C. D. (2018). Transposable elements generate regulatory novelty in a tissue-specific fashion. *BMC Genomics*, *19*(1). https://doi.org/10.1186/s12864-018-4850-3

Trizzino, M., Park, Y. S., Holsbach-Beltrame, M., Aracena, K., Mika, K., Caliskan, M., Perry, G. H., Lynch, V. J., & Brown, C. D. (2017). Transposable elements are the primary source of novelty in primate gene regulation. *Genome Research*, *27*(10), 1623–1633. https://doi.org/10.1101/gr.218149.116

Wang, H., Xing, J., Grover, D., Hedges Kyudong Han, D. J., Walker, J. A., & Batzer, M. A. (2005). SVA elements: A hominid-specific retroposon family. *Journal of Molecular Biology*, *354*(4), 994–1007. https://doi.org/10.1016/j.jmb.2005.09.085

Wang, J., Xie, G., Singh, M., Ghanbarian, A. T., Raskó, T., Szvetnik, A., Cai, H., Besser, D., Prigione, A., Fuchs, N. V., Schumann, G. G., Chen, W., Lorincz, M.

903 C., Ivics, Z., Hurst, L. D., & Izsvák, Z. (2014). Primate-specific endogenous
904 retrovirus-driven transcription defines naive-like stem cells. *Nature*, *516*(7531),
905 405–409. https://doi.org/10.1038/nature13804
906 Wray, G. A. (2007). The evolutionary significance of cis-regulatory mutations. *Nature*
907 *Reviews Genetics*, *8*(3), 206–216. https://doi.org/10.1038/nrg2063

908

909

910 **Figure legends**

911 **Figure 1. An inducible CRISPRi tool to repress human-specific SVAs and LR5Hs in**
912 **iPSC-derived CNCCs – (a)** Schematic overview of SVA and LTR5Hs transposable elements,
913 illustrating their structure and phylogenetic distribution across Old World monkeys, apes, and
914 humans. Human-specific SVA subfamilies (i.e., SVA_E/F/F1) and the LTR5Hs are highlighted,
915 along with the approximate number of elements in each category. **(b)** CRISPR-dCas9-KRAB
916 targeting strategy for SVAs and LTR5Hs. Two guide RNAs (gRNA1 and gRNA2) target ~80%
917 of all SVAs and LTR5Hs, directing dCas9-KRAB to deposit repressive epigenetic marks at the
918 TEs, thereby reducing their transcriptional activity. **(c)** Experimental timeline for doxycycline
919 (dox)-induced expression of dCas9-KRAB. Dox is added to the media 24 hours after the start
920 of differentiation into cranial neural crest cells, which spans 5 days. **(d)** Western blot confirming
921 dox-inducible dCas9-KRAB expression. Lysates from cells cultured with or without TE-
922 targetting gRNAs were probed with antibodies against dCas9 (top band, ~160 kDa) and
923 GAPDH (bottom band, loading control). **(e)** Immunofluorescence displaying expression of
924 CNCC signature markers AP2α (red) and SOX9 (green) in CNCCs differentiated using
925 CRISPRi-iPSCs without (left) and with gRNAs (right). Signal intensity was quantified and
926 normalised to the cell number per frame. This experiment was repeated at least once. **(f)** RT-
927 qPCR of CNCC markers *SOX9*, *TWIST1*, *SOX10* and *TFAP2A*. n=6: each data point is derived
928 from 6 independent rounds of NCC differentiation. Statistical analyses were performed using
929 unpaired t-tests. Error bars indicate mean ± SEM. ***, p=0.0002.

930 **Figure 2 – Hundreds of human-specific SVAs and LTR5Hs function as enhancers in**
931 **human CNCCs – (a)** ATAC-seq signal across human-specific SVAs and LTR5Hs. Heatmap
932 rows represent individual transposable elements (TEs) aligned at their start or end (±500 bp),
933 and the intensity reflects chromatin accessibility. Clusters were generated with deepTools
934 using k-mer algorithm. Two independent replicates per group. **(b)** Pie charts showing the
935 observed versus expected fractions of accessible TEs belonging to the LTR5Hs/SVA
936 subfamilies. **(c)** H3K9me3 enrichment at the accessible human-specific SVAs and LTR5Hs.
937 The top panel displays the average H3K9me3 signal (average profile) aligned to the TE start

938 or end (±3 kb), while the heatmap below shows individual TEs ranked by signal intensity. **(d)**
939 Transcription factor motif analysis of accessible human-specific SVAs and LTR5Hs.
940 Representative enriched motifs (TWIST1, HOMEOBOX, SOX9/10, AP2α, SLUG, and FOXD3)
941 in accessible human-specific TEs are shown with the percentage of TEs containing each motif.
942 **(e)** Heatmaps of TWIST1 ChIP-seq signal (left) and corresponding input control (right) centred
943 on the accessible human-specific SVAs and LTR5Hs (±2 kb). Colour intensity indicates
944 normalized enrichment, highlighting TWIST1 occupancy at these accessible elements.
945
946 **Figure 3. Human-specific SVAs and LTR5Hs regulate the expression of CNCC migration**
947 **genes – (a)** Violin plots displaying expression (log2 TPM) of genes located near accessible
948 human-specific SVAs and LTR5Hs. Three conditions are shown: human CNCCs generated
949 using CRISPRi iPSC line without guide RNAs (−gRNA), human CNCCs generated using
950 CRISPRi iPSC line with guide RNAs (+gRNA), and chimpanzee CNCCs. The decreased
951 expression in the +gRNA condition indicates potential regulatory contributions of these human-
952 specific TEs. **(b)** Volcano plot illustrating differentially expressed genes between the −gRNA
953 (n=3) and +gRNA (n=2) conditions in human CNCCs. The x-axis shows the log2 fold change,
954 while the y-axis represents the −log10 P-value. Significantly upregulated (green) and
955 downregulated (red) genes are highlighted, with total numbers indicated. Dashed lines mark
956 common significance thresholds. **(c)** Functional enrichment analysis of downregulated genes.
957 Bubble plots display top enriched pathways, with the x-axis indicating enrichment ratio (blue)
958 or the -log10 FDR (red) and the y-axis listing pathway terms. The size of each bubble reflects
959 statistical significance. Pathways involved in cell migration and motility are among the most
960 prominently enriched.
961
962 **Figure 4. HiPSC-NCCs show inferior migration capability when human-specific TEs are**
963 **silenced. (a)** Outline of the transwell migration assay. **(b)** 1 x 10^5 hiPSC-NCCs (+/- gRNAs)
964 were seeded overnight, followed by a media change in the upper chamber and incubation with
965 differentiation medium +10% FBS in the lower chamber for 24h. At 24h, non-migrated hiPSC-
966 NCCs on the top of the membrane were swabbed away and migrated hiPSC-CMs were fixed,
967 stained and imaged. DAPI staining was used to visualise nuclei. Scale bar: 50 μm. **(c)**
968 Quantification of transwell membranes. 10X images were taken from 4 different fields of view
969 and the average number of migrated cells was calculated. n=5. ***,p= 0.0008. **(d)** 5 x 10^4
970 hiPSC-NCCs (+/- gRNAs) were seeded overnight onto a 24-well plate. The next day, scratch
971 wounds were made and the hiPSC-NCCs were incubated with differentiation medium + 10%
972 FBS. After 8h, scratch wounds were imaged and wound closure was measured. n=12 (-
973 gRNAs), n=11 (+gRNAs). Scale bar: 200 μm. **(e)** Quantification of scratch wound closure was
974 performed with an automated plugin (Suarez-Arnedo et al., 2020). ****,p= 2.56×10^{-6}. Both

975 assays were independently performed twice. Statistical analyses were performed using an
976 unpaired t-test. Error bars indicate mean ± SEM.
977
978 **Figure 5. Enhancer signature of SVAs and LTR5Hs is cell-type specific –** Heatmaps of
979 normalized H3K27ac ChIP-seq signal (Roadmap Epigenomics Consortium) across 256
980 accessible human-specific SVAs and LTR5Hs in multiple tissues and cell types. Each row
981 corresponds to an individual transposable element (TE), aligned at its centre (±3 kb), while
982 columns represent different tissues/cell lines. The colour bar on the right indicates the relative
983 intensity of H3K27ac signal, with higher enrichment in red and lower enrichment in blue.

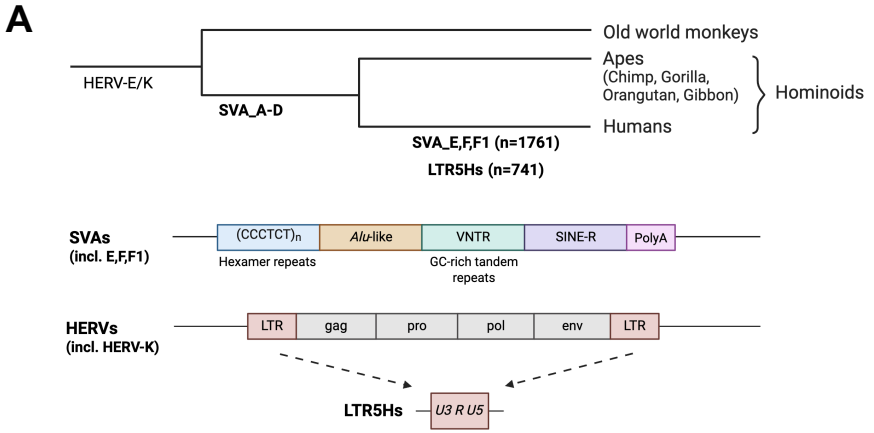
A
Old world monkeys
Apes
(Chimp, Gorilla, Orangutan, Gibbon)
Hominoids
Humans
HERV-E/K
SVA_A-D
SVA_E,F,F1 (n=1761)
LTR5Hs (n=741)
SVAs
(incl. E,F,F1)
(CCCTCT)n
Alu-like
VNTR
SINE-R
PolyA
Hexamer repeats
GC-rich tandem repeats
HERVs
(incl. HERV-K)
LTR
gag
pro
pol
env
LTR
LTR5Hs
U3 R U5

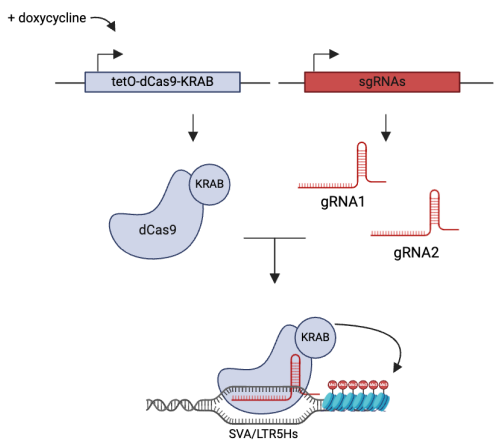
B
+ doxycycline
tetO-dCas9-KRAB
sgRNAs
KRAB
dCas9
gRNA1
gRNA2
KRAB
SVA/LTR5Hs

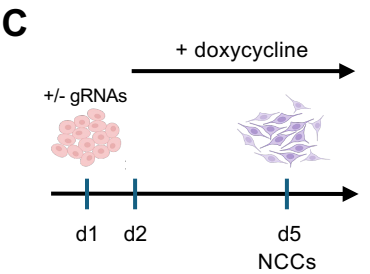
C
+ doxycycline
+/- gRNAs
d1
d2
d5
NCCs

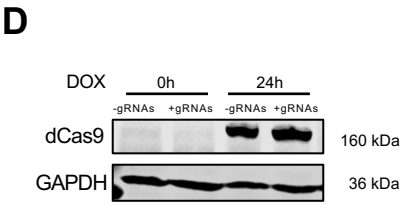
D
DOX
0h
24h
-gRNAs
+gRNAs
-gRNAs
+gRNAs
dCas9
160 kDa
GAPDH
36 kDa

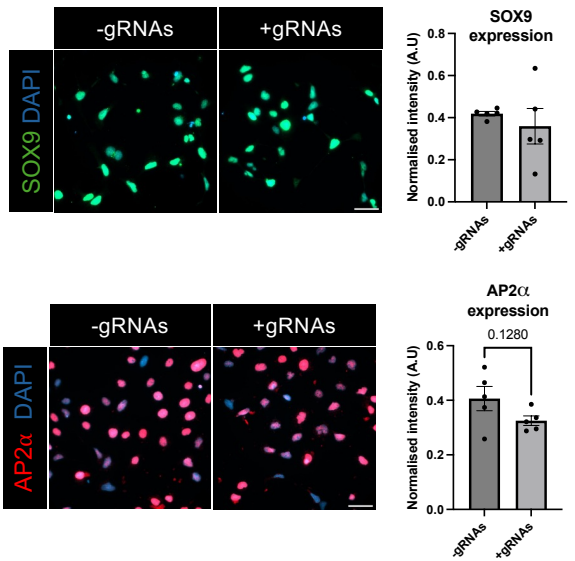
E
-gRNAs
+gRNAs
SOX9 DAPI
SOX9 expression
Normalised intensity (A.U)
-gRNAs
+gRNAs
-gRNAs
+gRNAs
AP2α DAPI
AP2α expression
0.1280
Normalised intensity (A.U)
-gRNAs
+gRNAs

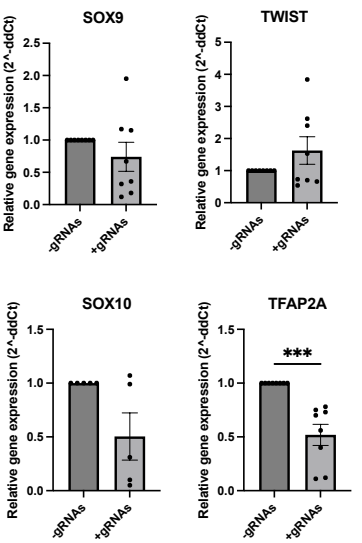
F
SOX9
TWIST
SOX10
TFAP2A
Relative gene expression (2^-ddCt)
***
-gRNAs
+gRNAs

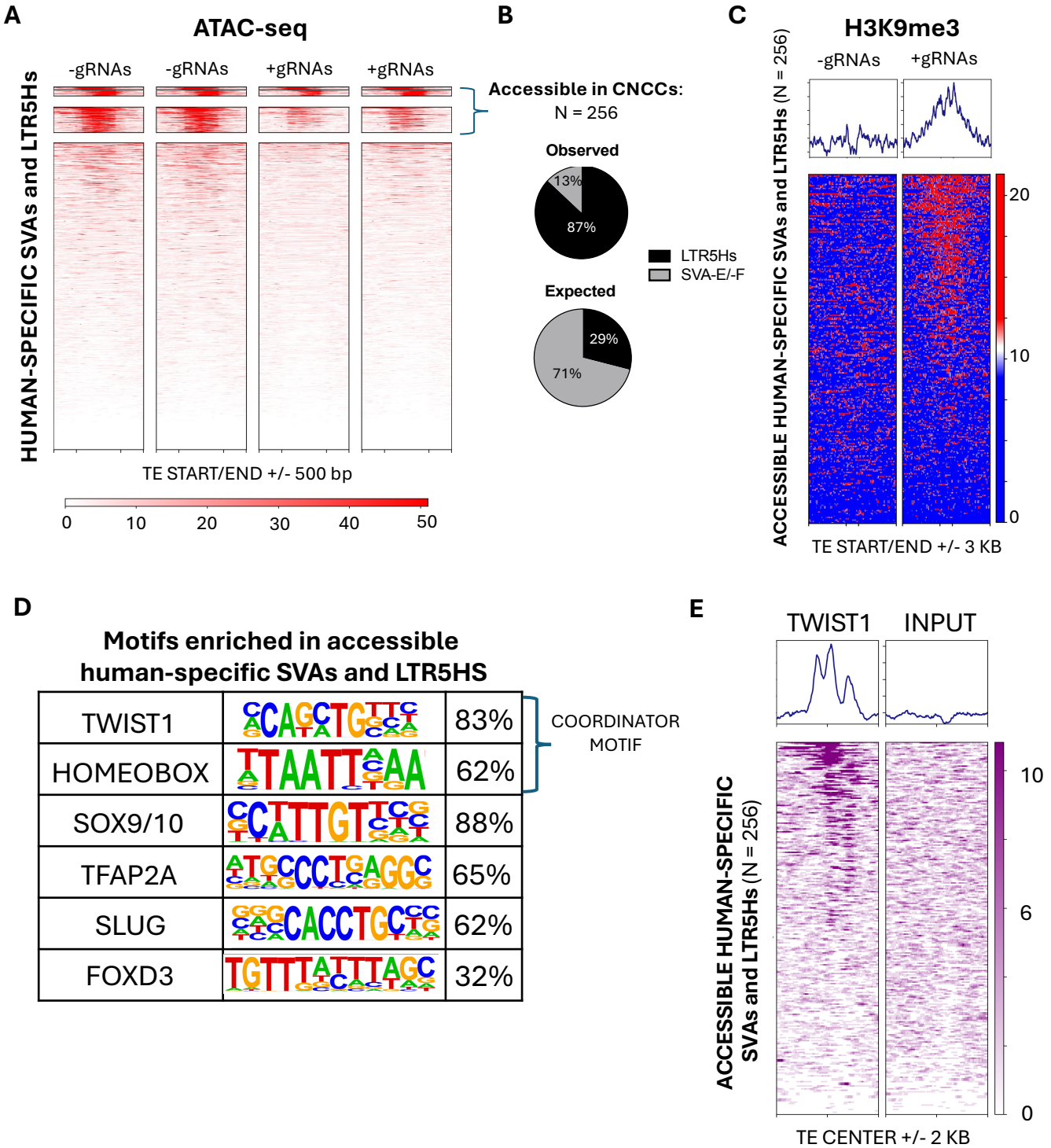
A
ATAC-seq
-gRNAs
-gRNAs
+gRNAs
+gRNAs
HUMAN-SPECIFIC SVAs and LTR5Hs
TE START/END +/- 500 bp
0
10
20
30
40
50
B
Accessible in CNCCs:
N = 256
Observed
13%
87%
Expected
29%
71%
LTR5Hs
SVA-E/-F
C
H3K9me3
-gRNAs
+gRNAs
ACCESSIBLE HUMAN-SPECIFIC SVAs and LTR5Hs (N = 256)
20
10
0
TE START/END +/- 3 KB
D
Motifs enriched in accessible human-specific SVAs and LTR5HS
TWIST1
83%
HOMEOBOX
62%
SOX9/10
88%
TFAP2A
65%
SLUG
62%
FOXD3
32%
COORDINATOR MOTIF
E
TWIST1
INPUT
ACCESSIBLE HUMAN-SPECIFIC SVAs and LTR5Hs (N = 256)
10
6
0
TE CENTER +/- 2 KB

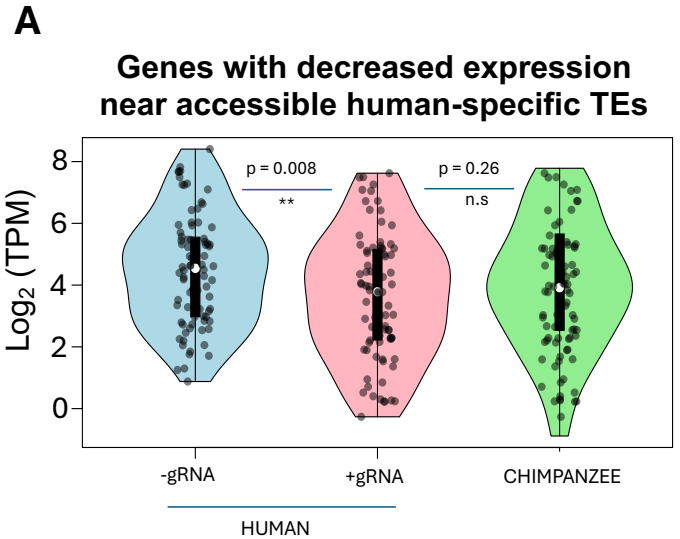
A
Genes with decreased expression
near accessible human-specific TEs
Log2 (TPM)
8
6
4
2
0
p = 0.008
**
p = 0.26
n.s
-gRNA
+gRNA
CHIMPANZEE
HUMAN

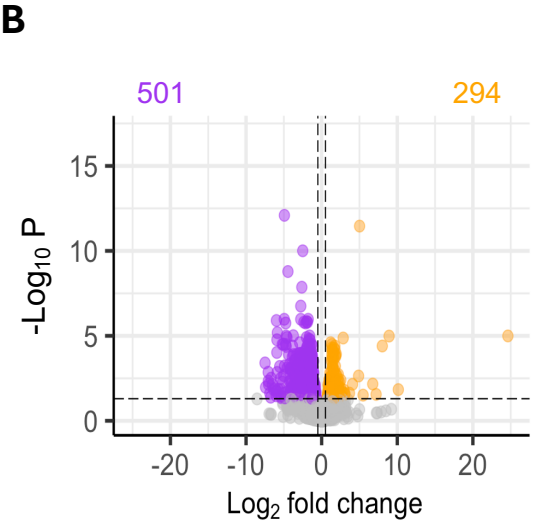
B
501
294
-Log10 P
15
10
5
0
-20
-10
0
10
20
Log2 fold change

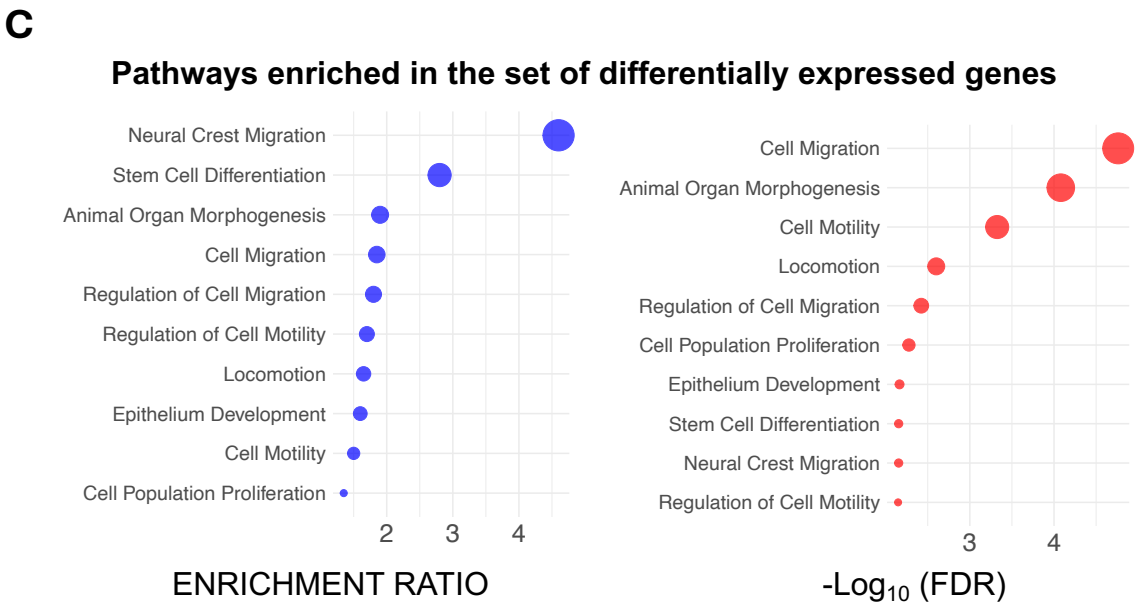
C
Pathways enriched in the set of differentially expressed genes
Neural Crest Migration
Stem Cell Differentiation
Animal Organ Morphogenesis
Cell Migration
Regulation of Cell Migration
Regulation of Cell Motility
Locomotion
Epithelium Development
Cell Motility
Cell Population Proliferation
2
3
4
ENRICHMENT RATIO
Cell Migration
Animal Organ Morphogenesis
Cell Motility
Locomotion
Regulation of Cell Migration
Cell Population Proliferation
Epithelium Development
Stem Cell Differentiation
Neural Crest Migration
Regulation of Cell Motility
3
4
-Log10 (FDR)

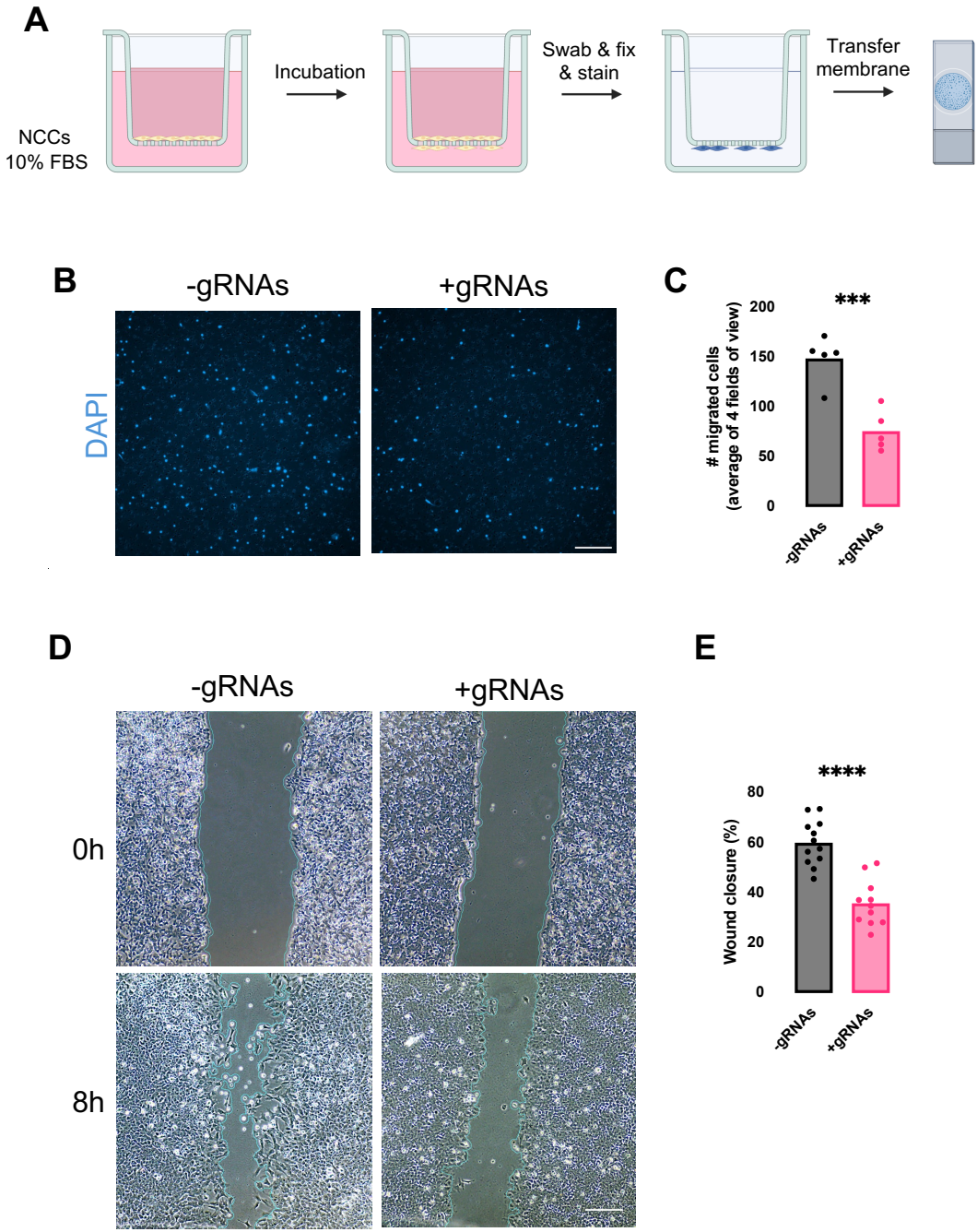
A
NCCs
10% FBS
Incubation
Swab & fix
& stain
Transfer
membrane
B
-gRNAs
+gRNAs
DAPI
C
***
migrated cells
(average of 4 fields of view)
200
150
100
50
0
-gRNAs
+gRNAs
D
-gRNAs
+gRNAs
0h
8h
E
****
Wound closure (%)
80
60
40
20
0
-gRNAs
+gRNAs

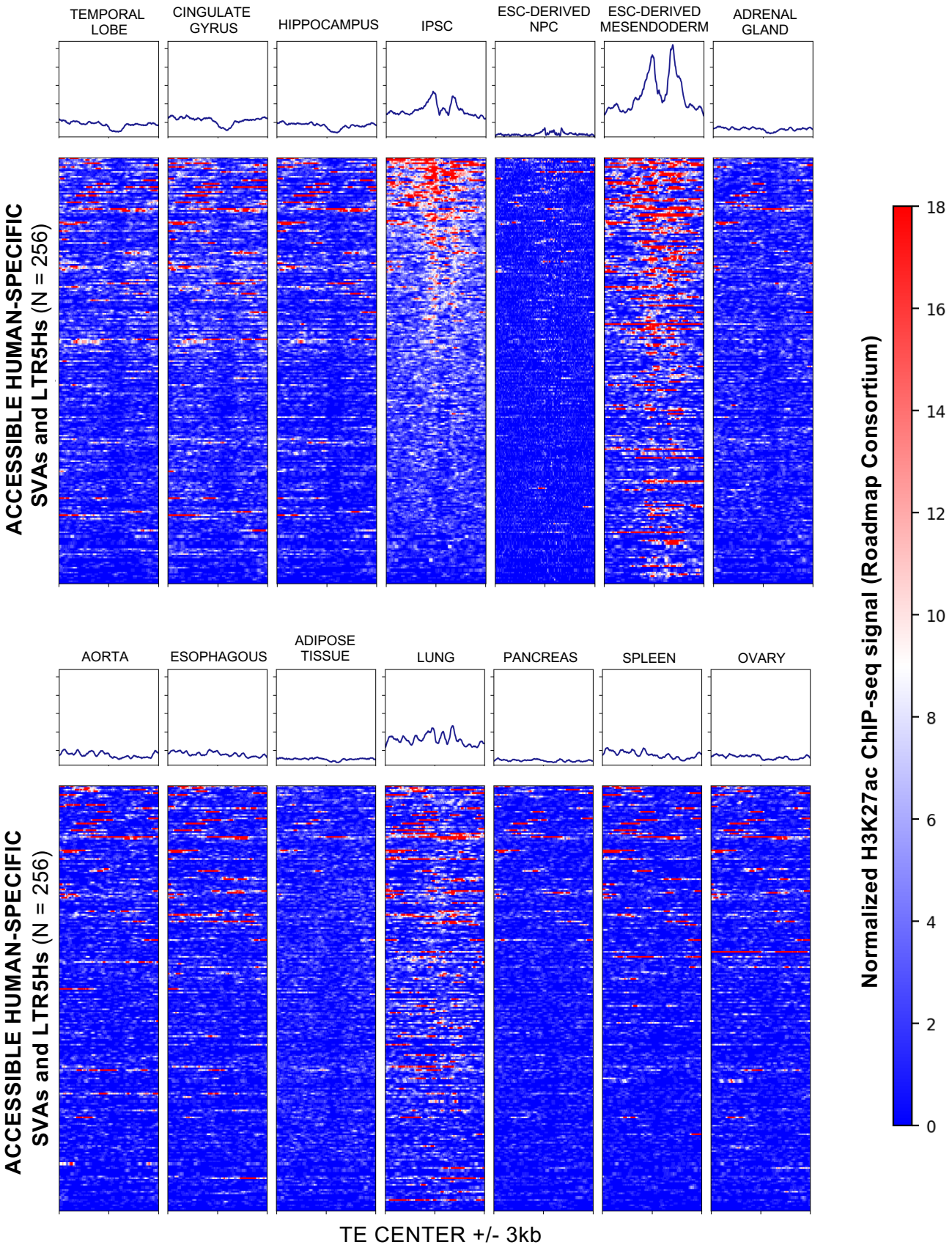
TEMPORAL LOBE
CINGULATE GYRUS
HIPPOCAMPUS
IPSC
ESC-DERIVED NPC
ESC-DERIVED MESENDODERM
ADRENAL GLAND
ACCESSIBLE HUMAN-SPECIFIC SVAs and LTR5Hs (N = 256)
AORTA
ESOPHAGOUS
ADIPOSE TISSUE
LUNG
PANCREAS
SPLEEN
OVARY
ACCESSIBLE HUMAN-SPECIFIC SVAs and LTR5Hs (N = 256)
TE CENTER +/- 3kb
Normalized H3K27ac ChIP-seq signal (Roadmap Consortium)
18
16
14
12
10
8
6
4
2
0